

PRELIMINARY EVALUATION OF A MEMS-BASED WATER PROPELLANT VAPORIZING LIQUID MICROTHRUSTER FOR SMALL SATELLITES

M.G. De Giorgi^{1*}, D. Fontanarosa¹, L. Francioso², C. De Pascali² and A. Ficarella¹

¹Dept. of Engineering for Innovation, University of Salento, Via per Monteroni “Campus Ecotekne”, LECCE I-73100, Italy

²Institute for Microelectronics and Microsystems IMM-CNR, Via per Monteroni “Campus Ecotekne”, LECCE I-73100, Italy

*corresponding author: mariagrazia.degiorgi@unisalento.it

ABSTRACT

In the space field, the recent advancement in the Micro-Electric-Mechanical Systems (MEMS) technology has allowed for the development of small satellites (total mass less than 20 kg), thanks to the reduction of the total expenditure of space missions under Low Earth Orbit (LEO). Micro- and nano-satellites usually require very small thrust forces in order to ensure the orbit and/or attitude control, from few micro-newtons up to some milli-newtons, in combination with stringent constraints of mass, volume and power consumption to be satisfied.

Therefore, the micro-propulsion system represents a key technology, and water-propellant micro-resistojets provide a green and reliable solution in the class of electric propulsion. The present work first describes the final design of a low-cost, flexible, silicon-based water-propellant vaporizing liquid microthruster (VLM) prototype. The VLM composes of an inlet chamber, a set of parallel microchannels as heating chamber, and a planar convergent-divergent micronozzle. The microthruster has a sandwich structure. The inlet chamber, the heating chamber and the micronozzle have been fabricated using anisotropic wet etching of a silicon substrate coupled with specialty Borofloat 33® glass. The Borofloat wafer was coupled to silicon wafer by thermocompressive bonding, which allowed to ensure one optical access to the flow field inside the microthruster. A Platinum resistive film placed on the bottom of the silicon pad provides the heat required for vaporization and superheating. In addition, the microthruster is equipped with sensing capabilities for the temperature and the vapor quality, thanks to a of thermistors and capacitive sensors which are embedded on the device.

Based on experimental tests at ambient conditions focused on both the propulsive and the sensing items, a preliminary assessment of the operational feasibility of the microthruster at ambient conditions has been provided. The experimental investigation has been supported by a numerical investigation for the performance prediction under vacuum conditions using a one-dimensional model of the microthruster. In addition, 2D CFD simulations have been performed in order to estimate the impact of the gas rarefaction on the propulsive performance of the micro-thruster and provide a description of the flow inside the micronozzle. To this purpose, continuous Navier-Stokes simulations under slip regime condition has been carried out which results have been compared with those retrieved by the one-dimensional modeling.

Keywords: Micro propulsion, micro-resistojets, vaporizing liquid microthruster, small satellites

1 INTRODUCTION

In the last twenty years, the efforts of the scientific community have gone into research and development of cubesats with total mass less than 20 kg. These satellites have to be equipped with the micro-propulsion system capable to provide small thrust forces from μN to some mN in compliance with stringent constraints of mass, volume and power consumption. In addition, the use of green propellants in place of the traditional toxic bi-/mono-propellants such as hydrazine, represents another relevant requirement for micro-propulsion system.

The recent developments in microthruster technology have benefit from the advancement in Micro-Electric-Mechanical Systems (MEMS) machining. We refer to [1] for a detailed review of micro-propulsion systems applied to small satellites. In the field of the micro-propulsion, micro-resistojets represent an interesting choice they are currently able to satisfy all mass, volume and power constraints and provide thrust levels requirements required for the attitude control and the pointing systems of miniaturized spacecrafts [2][3][4]. Devices that use liquid propellants are called Vaporizing Liquid Microthrusters (VLMs), which can store the propellant in low pressure and light weight fuel tank in comparison with cold/hot gas micro-thrusters, even though they will consume more electric power due to the evaporation process.

The early development concerning VLMs dates back to the Mueller's studies [[5],[6],[7]]. He first designed and manufactured a silicon-based MEMS device, characterized the heat losses in relation to the packaging, and investigated the influence of feeding pressure on the vaporization process. Later, Makherjee et al. [8] used wet anisotropic etching to fabricate a water propellant MEMS-based micro-thruster, and they measured thrust force magnitudes ranging between 0.15-0.46 mN. Using water as propellant, Maurya et al. [9] designed a silicon-based VLM with integrated micro-heater, which demonstrated to be able to provide thrust forces in the range 5 to 20 μN with heating power between 1 W and 2.4 W. Instead, a single-channel VLM equipped with two integrated heaters was manufactured and tested by Kundu et al. [10]. Their thruster generated thrust force of about 1 mN using maximum heater power of 3.6 W. Ye et al. [11] implemented pulsated heating by means of the application of an electric pulse. Their micro-thruster exhibited a total impulse of 0.2 Ns with pulse power of 30 W. More recently, Silva et al. [3] integrated molybdenum heaters and temperature sensing using water as green propellant into a VLM in compliance with the strict requirements of small satellites programs. Concerning new materials and manufacturing technologies, Karthikeyan et al. [12] first manufactured a low temperature co-fired ceramic (LTCC) VLM, demonstrating the advantages in using the LTCC in place of the silicon (i.e. good electrical conductivity of printed metallization, a relative low cost for mass production, and a relatively simple and fast fabrication process). Later, Cheah and Low [13] proposed a high temperature co-fired ceramic (HTCC) VLM made by a three layers structure with a platinum-based microheater.

Furthermore, the establishment of micro-flow boiling instabilities inside the microchannels of the heating chamber usually affects the overall performance of the VLMs. In this regard, Chen et al. [14] first investigated the two-phase flow characteristics in a single channel silicon-based VLM, and identified four different flow patterns. Later, Cen and Xu [15] characterized the flow boiling instabilities in relation to the measured performance inside a MEMS-based VLM made by parallel microchannels. Moreover, the growth of the viscous boundary layer inside planar micronozzles, enhanced by the micro-scale and the rarefied gas condition, is worth to be considered since it strongly affects the propulsive efficiency of this kind of microthrusters.

In this context, both the geometry optimization and embedded sensing capability play a crucial role in controlling the heating process and the behavior of the two-phase flow, which allows to mitigate the efficiency losses and hinder the fluid-induced instabilities. The present work aims to present the design of a VLM concept which is equipped with temperature and void fraction sensors, and a secondary fine-heating system. Furthermore, the baseline configuration is made of parallel rectangular microchannels, yet several geometry modifications have been considered

in order to reduce the flow boiling instabilities. Preliminary tests at ambient pressure have been carried on the first prototype of the device, which demonstrated the operational functioning of the overall microthruster as well as the integrated temperature sensing. Hence, based on experiments, the propulsive performance under vacuum conditions have been predicted by means of a one-dimensional model and 2D CFD computations of the supersonic flow inside the micronozzle.

2 DEVICE DESCRIPTION AND FABRICATION

A 3D schematic of the vaporizing liquid microthruster is shown in Figure 1. It consists of three regions:

- an inlet chamber or plenum through which the propellant is fed;
- the heating chamber where the propellant is vaporized;
- a planar convergent-divergent micronozzle which accelerates the superheated vapor flow to supersonic velocities.

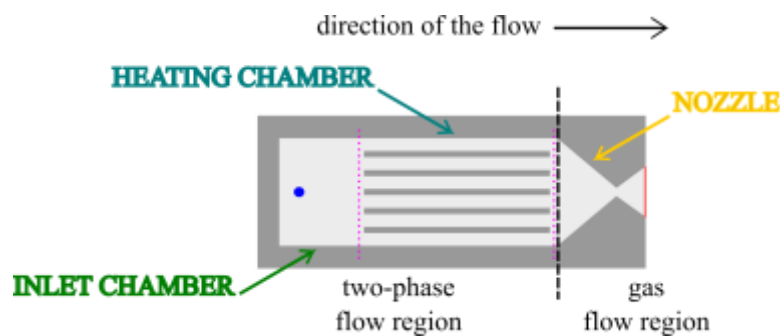


Figure 1: MEMS schematics of the microthruster

As shown in Figure 2, the VLM has a sandwich structure: the inlet chamber, the heating chamber and the micronozzle are realized by deep silicon anisotropic etching, coupled with a Borofloat 33® glass wafer that ensures fluidic tightness, optical access to the flow field inside the microthruster channels and sensor integration.

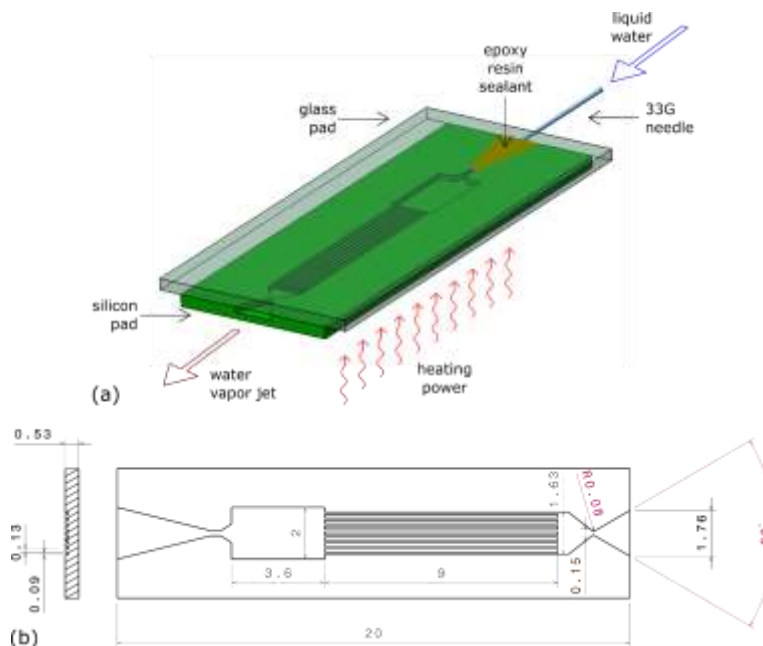


Figure 2: Concept of the vaporizing liquid microthruster: (a) 3D schematic view; (b) 2D drawing of the silicon pad (units are in millimetre).

A thin film Platinum heater placed on the bottom of the silicon substrate provided the heat to the propellant fluid. Furthermore, a set of capacitive void fraction sensors (VFSs) and 4-wires resistance temperature detectors (RTDs) equipped the device, with the aim to provide sensing capabilities for the flow control inside the microthruster. Furthermore, secondary resistive heaters have been patterned by photolithography on the glass substrate as low-power heating for flow control test. The MEMS schematics in Figure 3 highlights the configuration of sensors and heaters.

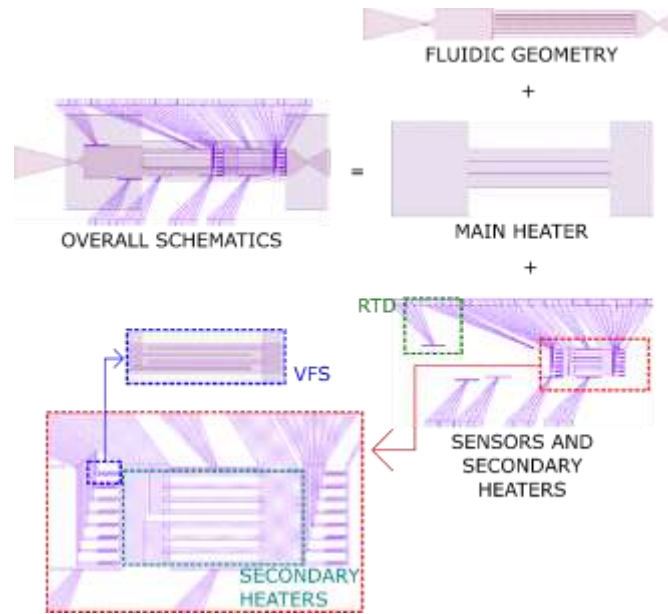


Figure 3: MEMS schematics of the microthruster.

The microthrusters fabrication has been performed at the CNR-IMM clean room facilities, with a custom process design that integrates different pattern transfer techniques, vacuum depositions, deep dry etching of silicon, front-back lithography alignment steps and adhesive silicon-glass bonding. A picture of a microthruster prototype is shown in Figure 4 (a), while Figure 4 (b) displays the front and side views of the microthruster in its operative configuration with both feeding needle and electrical wirings of the main heater.

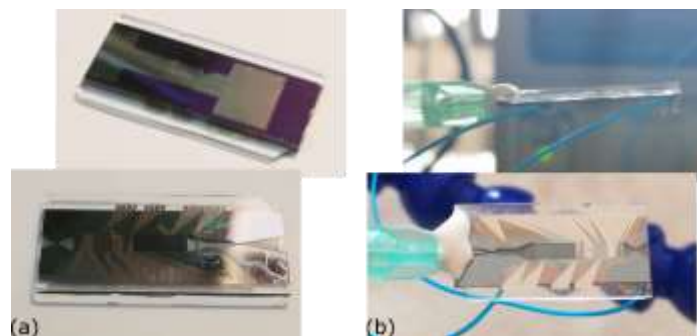


Figure 4: Picture of a VLM prototype: (a) top and bottom views of the manufactured device; (b) top and side views of the operative configuration equipped with the feeding needle and the electrical wire of the main heater.

Concerning the geometry of the thruster, the device has length of about 20 mm, width of 7 mm and total thickness of about 500 μm , while the etching depth for channel definition is about 230 μm . The length and the thickness of glass pad are equal to the ones of the silicon substrate, while it is 9 mm width in order to allow placement of the connection pads and secondary heaters

the electrical pads of sensors and secondary heaters. A V-shaped inlet of about 2 mm length ensures water feeding inside the chip using a 33G needle, which is fixed to the device by means of an epoxy resin that provides the proper junction tightness. Eight microchannels of 90 μm width and 9 mm length compose the heating chamber, which should ensure the maximization of the heat transfer coefficient, the reduction of the pressure losses and the hindering of flow boiling instabilities. Microchannels are spaced apart of 130 μm each other. Concerning the convergent-divergent planar micronozzle, its throat width is about 150 μm , the angle of the convergence section is about 45° , while the divergent section owns 30° . The choice of a high divergence angle is related to the mitigation of the viscous losses due to the boundary layer growth normal to the planar walls, as demonstrated in [16].

The trade-off between performance, safety, and any other desired features such as density, heat capacity, safety, storability and availability, usually lead to the choice of the propellant. Based on the analysis performed by [19], water has been selected as the propellant for use in the present VLM as a result of the comparison between four parameters: the increment of velocity per unit volume $\Delta V/V$, the specific impulse I_{sp} , the electrical power needed for vaporization $P_{el,v}$, and the safety issue. In particular, water ensures an ultra-safe operational environment, as well as it is environmentally friendly and cheap, it has high density and it is stable enough to be stored in a weakly pressurized light tank. A greater power consumption due to the high enthalpy of vaporization is the most relevant drawback, yet it can still meet the expected requirements for small satellites.

3 NUMERICAL PREDICTIVE ANALYSIS

The one-dimensional model of the VLM, which was proposed and validated by the authors in [18], has been applied to the present configuration. It allows to describe the behaviour of the liquid–vapor flow inside the inlet and the heating chambers of the microthruster, based on the hypothesis of thin film flow and considering the 1D approximation [19]. The toolbox CoolProp [20] is integrated into the code to compute the two-phase mixture properties.

The heating process begins into the inlet chamber at the end of which the flow enters the microchannels region. The model computes the variation of the total enthalpy of the flow across a spatial step Δs as follows:

$$\Delta H = \dot{Q} \Delta t = \dot{q} P_{cs} \Delta s = [h_b(T_w - T)] P_{cs} \Delta s \quad (1)$$

where Δt is the time step, T_w is temperature of the inner wall, \dot{Q} is the heat power exchanged between the fluid and the silicon walls and P_{cs} is the perimeter of the cross section. The heat flux \dot{q} is related to the convective heat exchange driven by the heat transfer coefficient $h_b = Nu (\kappa_{cond}/D_h)$, where κ_{cond} is the local thermal conductivity coefficient of the fluid and D_h is the hydraulic diameter. Instead, the Nusselt number Nu is locally estimated based on the empirical correlations extrapolated by Tibiriçá et al. [21]. As a result, the local heat transfer coefficient is estimated as in Eq. (4):

$$h_b = \begin{cases} \frac{Nu(x) \kappa_{cond}}{D_h}, & x < x_{d/o} \\ \frac{Nu(x) \kappa_{cond}}{D_h} - 0.5 \left[\frac{Nu(x) \kappa_{cond}}{D_h} - h_{b,DB} \right] \frac{(x - x_{d/o})}{(1 - x_{d/o})}, & x \geq x_{d/o} \end{cases} \quad (2)$$

where $x_{d/o}$ represents the vapor quality at the dry-out condition, while the local Nusselt number and the Dittus–Boelter super-heated vapor relation are defined in Eqs. (3) and (4):

$$Nu(x) = \begin{cases} 0.68 Pr^{0.5414} La^{0.1942} Re^{0.5873} (1 - x)^{-0.2446} Bo^{0.3544}, & x < x_{d/o} \\ 0.68 Pr^{0.5414} La^{0.1942} Re^{0.5873} (1 - x_{d/o})^{-0.2446} Bo^{0.3544}, & x \geq x_{d/o} \end{cases} \quad (3)$$

$$h_{b,DB} = 0.023 \frac{\kappa_{v,cond}}{D_h} Re_v^{0.8} Pr_v^{1/3} \quad (4)$$

In equations above, Re_v and Pr_v , respectively are the local Reynolds and Prandtl numbers of the vapor phase.

The prediction of the microthruster performance in terms of thrust and specific impulse is based on the ideal rocket theory (IRT). The maximum mass flow rate \dot{m}_{IRT} was estimated by supposing choked flow conditions at the throat section of the micronozzle as follows:

$$\dot{m}_{IRT} = \Gamma_{VDK} \frac{p_0 A^*}{\sqrt{R_{gas} T_0}} \quad (5)$$

where p_0 and T_0 are the stagnation pressure and temperature at the exit of microchannels, p_{exit} is the static pressure at the exit section and A^* is the area at the throat section. Furthermore, the velocity of the supersonic flow at the exit section is

$$u_{exit,IRT} = \sqrt{\frac{2\gamma R_{gas} T_0 p_0 A^*}{\gamma - 1} \left[1 - \left(\frac{p_{exit}}{p_0} \right)^{\frac{\gamma-1}{\gamma}} \right]} \quad (6)$$

where R_{gas} is specific gas constant, $\Gamma_{VDK} = \left[\gamma \left(\frac{2}{\gamma - 1} \right)^{\frac{\gamma+1}{\gamma-1}} \right]^{1/2}$ is the Vanderkerchoff factor, γ is the specific heat ratio of the propellant. Therefore, the thrust and the specific impulse result from Eqs. (9) and (10),

$$F_{IRT} = F_{j,IRT} + F_{p,IRT} = \dot{m}_{IRT} u_{exit,IRT} + (p_{exit} - p_{amb}) A_{exit} \quad (7)$$

$$I_{sp,IRT} = \frac{F_{IRT}}{\dot{m}_{IRT} g_0} = \frac{u_{eff}}{g_0} \quad (8)$$

where the subscripts j and p denote the momentum thrust and the pressure thrust respectively, and u_{eff} is the effective exhaust velocity which takes account of both thrust terms, p_{amb} is the farfield ambient pressure.

The establishment of the boundary layer at the nozzle throat and along the divergent section of the micronozzle reduces both the mass flow rate and the exit velocity. Hence, the micronozzle quality ξ_n has been considered in order to quantifies the total performance losses due to growth of the boundary layer thickness inside the micronozzle as follows:

$$F_{act} = \dot{m}_{act} u_{act} = (C_d \dot{m}_{IRT}) + (\eta_u u_{exit,IRT}) = (C_d \eta_u) \dot{m}_{IRT} u_{exit,IRT} = \xi_n F_{IRT} \quad (9)$$

where the subscript act denotes the actual performance, C_d is the discharge coefficient and η_u is the Isp-efficiency, In particular, C_d is related to the geometry of the nozzle throat, the propellant and the Reynolds number at the throat section, while η_u depends on both the compressible momentum and the displacement thicknesses as a measure of the the jet momentum reduction due to the difference between the inviscid and the viscous velocity inside the boundary layer. We refer to [20] for the detailed description of the model and for the operational range of validity of the experimental correlations regarding the two-phase flow behavior.

3.1 CFD modeling of the supersonic flow into the micronozzle

CFD simulations of the gas flow through the micronozzle were performed by using the open source CFD toolbox OpenFOAM© Version 3.0.1, based on a Finite Volume formulation. The density-based solver rhoCentralFoam [22] solved the Navier–Stokes (NS) equations in

combination with the laminar flow approximation in reference to the turbulence modeling. Concerning numerical schemes, the central upwind scheme of Kurganov and Tadmor was used for the flux terms and the Total Variation Diminishing (TVD) van Leer limiter for interpolation. The time step was determined based on a maximum Courant number Co_{max} of 0.2. In particular, the viscous governing equations were solved using a Preconditioned Conjugate Gradient/Diagonal Incomplete Cholesky scheme with a residual tolerance of 1×10^{-8} , while the inviscid equations of momentum and energy were explicitly solved by means of a Gauss–Siedel Smooth solver with a residual tolerance of 1×10^{-10} . The establishment of the steady state regime was ensured by monitoring the Mach number at mid-point of nozzle exit. The geometry of the micronozzle was based on the microthruster design previously described. Furthermore, a radius of curvature equal to $75 \mu\text{m}$ characterized the throat section, while eight inlets were defined corresponding to the exit section of microchannels, followed by a mixing region of $180 \mu\text{m}$ length before the entrance into the convergent region. The domain extended $15W_{exit}$ downstream and $6.5W_{exit}$ upward, where W_{exit} is the width of the exit section,

4 RESULTS AND DISCUSSION

4.1 Experimental characterization of the device

A custom experimental setup has been implemented for the characterization of the different sensors and actuators embedded into the microthruster. To this aim, different tests have been carried out to generate reliable calibration curve for the RTD sensors (for real temperature detection on chip), the main heater (for heating of the chamber and channels by Joule effect) and the capacitive void fraction sensors (VFSs) for vapour/liquid ratio identification.

In order to perform the preliminary analysis of the device properties, a set of experiments was carried out. The corresponding feeding pressures and the RTD measurements are reported in Figure 4 (a) and (b) respectively.

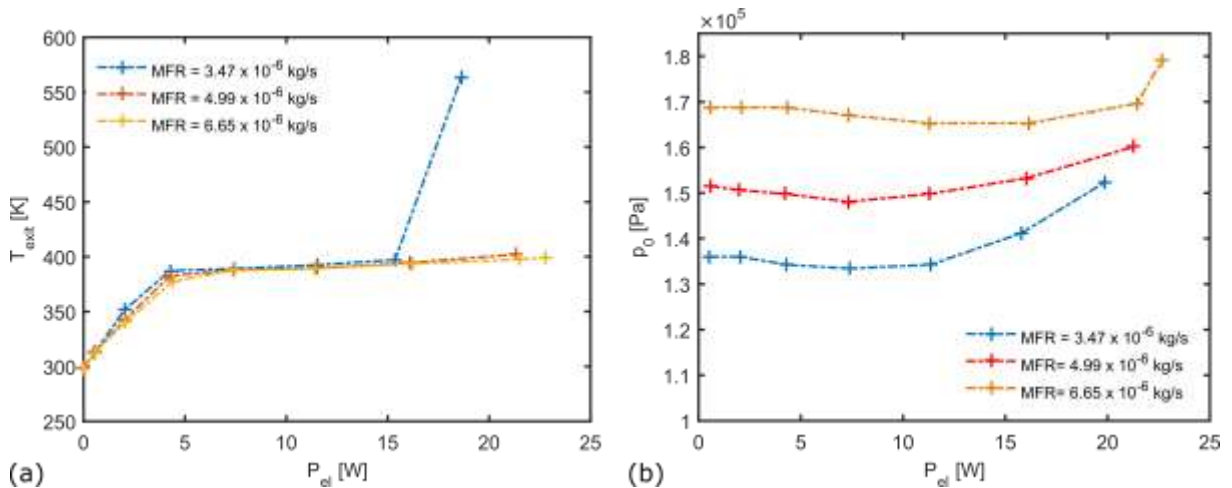


Figure 4. RTD measurements (a) and feeding pressure (b) as a function of the electrical power P_{el} and the mass flow rate (MFR).

In particular, three mass flow rates were considered, and flow observation, pressure and temperature measurements have been performed using the RTD placed close to the micronozzle, considering that the density of water at ambient condition is about 998.2 kg/m^3 . The experimental results for RTD without (empty configuration, at $\dot{m}=0 \text{ kg/s}$) and with water flow (propulsive configuration) are reported here below.

Figure 5 (a) reports the calibration of the RTD into a reference furnaces and the correlation between the experimental data (red cross) and the interpolation law. Once obtained this calibration for the RTD embedded into the devices, an experimental session has been focused on the collection of the vapour stream temperature vs the applied power to the main heater of the microthruster. As shown in Figure 5 (b), the applied voltage was correlated to an increasing Joule heating of the chip. The chip temperature increases as the power increase and a temperature plateau was recorded around 387 K. Further power increase caused a temperature spike and a rapid decrease to a stable value of about 400 K.

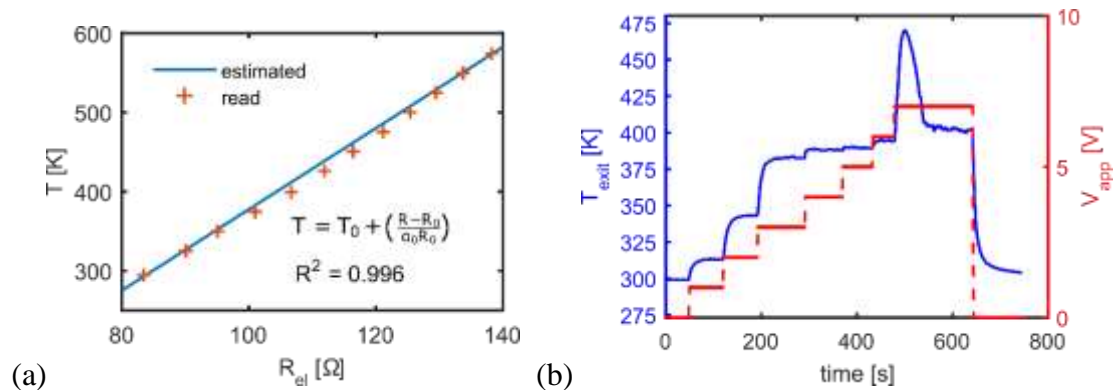


Figure 5: RTD characterization: (a) RTD calibration in the empty configuration at $\dot{m}=0$ kg/s ($\alpha_0=0.002337$, $R_0=83.51$ Ω , $T_0=293.15$ K); (b) RTD temperature measurement during 0-7 volts loading cycle in operative configuration at $\dot{m}=4.99 \times 10^{-6}$ kg/s ($\alpha_0=0.002337$, $R_0=84.5$ Ω , $T_0=297.15$ K).

In order to assess the validity of the measurement provided by the embedded RTD, the temperature of the microthruster was measured by means of a commercial thermistor (model PT1000) secured at the midpoint on the bottom side of the microthruster, at mass flow rate of 3.47×10^{-6} kg/s and different electrical powers. Temperature readings resulted from resistance-temperature conversion relationship in accordance with the standard IEC751/ITS-90. The measured data were compared with ones provided by the integrated RTD at the same mass flow rate, as shown in Figure 6. Even though the temperature measure provided by the embedded RTD was higher than those read through the sensor PT1000 (due to some thermal resistance at the interface between PT1000 sensors and chip surface), the two experimentally retrieved curve exhibited the same trend with good data fit. This result confirmed the reliability of the temperature sensing provided to the VLM by the integrated RTD.

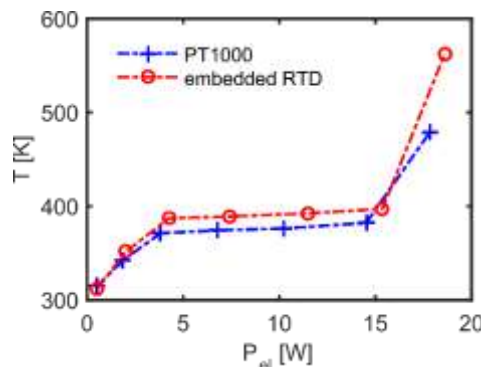


Figure 6: Temperature measurement provided by the integrated RTD (red line with circles) in comparison with the one provided by the sensor PT1000 (blue line with crosses).

4.2 Numerical prediction of propulsive performance

As evinced from the experimental data reported in Table 1, full evaporation with significant superheating of the vapor flow inside the microchannel was retrieved at mass flow rate of 3.47×10^{-6} kg/s and electrical power of 18.62 W. Hence, based on the temperature and pressure measurement, a preliminary estimation of the performance of the microthruster under vacuum condition was performed using the one-dimensional modeling previously described. In particular, the feeding pressure and the wall temperature were set to 1.52×10^5 Pa and 563.01 K, respectively, while water temperature at the microthruster entrance was assumed equal to 296.15 K. The far field pressure downstream the microthruster was supposed equal to 20 Pa. The solution of the two-phase flow inside the inlet chamber and microchannels is reported in Figure 7. Numerical prediction confirmed the complete evaporation of the flow, which would enter the micronozzle at a temperature of about 464 K and a total pressure of about 1.51×10^5 Pascal.

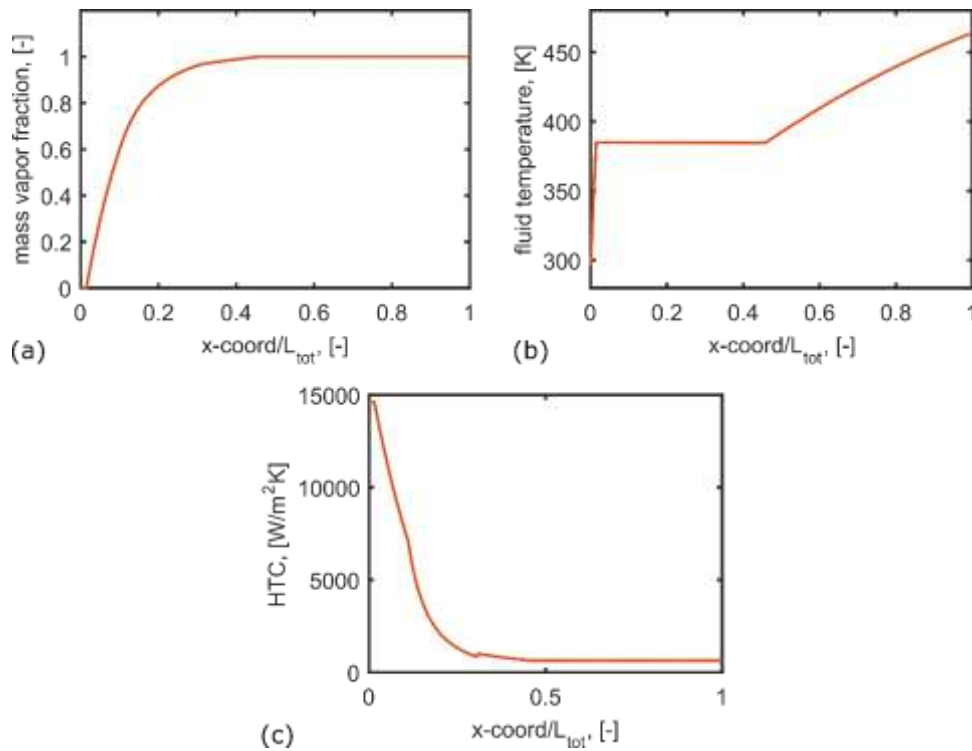


Figure 7. One-dimensional numerical prediction of the two-phase flow behavior inside the heating region (inlet chamber and microchannels): (a) vapor quality; (b) fluid temperature; (c) heat transfer coefficient (HTC). L_{tot} is the length of the heating region.

Based on the micronozzle inlet conditions estimated at the exit of the microchannels, the solution of the supersonic expansion was given. As a result, the mass flow rate should be increased to about 7.17×10^{-6} kg/s in order to ensure the choked flow condition at the throat section. Computations estimated a micronozzle quality ξ_n of 0.87 approximately. Therefore, the predicted net thrust would be about 7.7 mN, corresponding to a specific impulse of about 110 s. The solution provided by the 1D model was compared to the performance predicted by means of 2D CFD computations inside the micronozzle. To this purpose, the mass flow rate was set to 7.17×10^{-6} kg/s, the ambient pressure was set to 20 Pa, and the inlet temperature was fixed at 464 K in accordance with the temperature of the flow at the microchannel exit predicted by the 1D model. A partial slip boundary condition at walls was used since the maximum Knudsen number Kn into the divergent was strictly below 1×10^{-1} . In particular, a tangential momentum accommodation coefficient (σ_{TMAC}) of 0.80 was imposed using a first order Maxwell slip model

in reference of a generic gas flow on polished silicon microchannels. The CFD estimation of η_u was performed by comparing the thrust force resulting from the use of the Maxwellian slip, with the one obtained by setting the pure slip condition at wall at the same operating conditions, i.e. $\eta_u = F/F_{pureSlip}$. Instead, the discharge coefficient related to CFD computations was estimated from Eq. (5) by considering the average total pressure at the inlet predicted by CFD simulations, namely $C_d = \dot{m}/\dot{m}_{IRT}$. Results and comparisons are reported in Table 1, which highlights that the 2D CFD model overpredicts the microthruster performance since it does not consider the viscous losses related to the growth of the boundary layer thickness along the depthwise direction of the nozzle, as pointed out in [20]. Despite this, the 2D CFD model take account of the viscous losses due to the boundary layer growth along the widthwise direction, as shown in Figure 8.

Table 1. Test Matrix

Test case #	F [mN]	I _{sp} [s]	C _d [-]	η_u [-]	ξ_n [-]
1D model	7.7	109.8	0.950	0.917	0.87
2D CFD	8.3	117.6	0.956	0.982	0.94

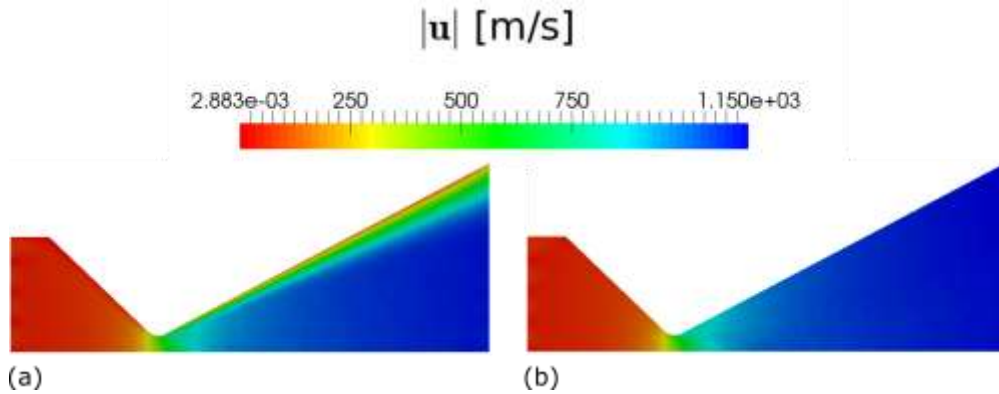


Figure 8. Contour of the velocity field predicted by 2D CFD computations: (a) partial slip condition at walls with $\sigma_{TMAC} = 0.80$; (b) pure slip condition at walls.

5 CONCLUDING REMARKS

The present work presented the development of a wafer-level fabrication of a micro-resistojet for attitude control of small satellites. The design and the fabrication of a silicon/glass water-propellant vaporizing liquid microthruster (VLM) were first described; therefore, the results of the operational characterization at ambient pressure of a device prototype was presented. Experimental results confirmed the functionality of the devices at different mass flow rates and supplied powers for Joule effect heating of the chip. The embedded RTD have been tested, calibrated and its measurements have been compared with those retrieved by using a commercial PT1000 thin film miniature sensors, with a good agreement of measured temperature near the VLM channels between the two sensors. Experiments also confirmed that the full evaporation with significant superheating of the vapor flow inside the microchannel was retrieved at mass flow rate of 3.47×10^{-6} kg/s and electrical power of 18.62 W. Based on this operating condition, a preliminary estimation of the performance of the microthruster under vacuum condition was performed using both the one-dimensional modelling and 2D CFD computations. The former predicted the behavior of the two-phase flow inside microchannels, as well as a real performance estimation of the micronozzle performance. In this regard, a micronozzle quality of 0.87 was estimated in combination with a net thrust of about 7.7 mN, corresponding to a specific impulse of about 110 s. Using the condition of the flow predicted by the 1D model at the exit of the microchannels, the 2D CFD simulations were initialized for

the solution of the supersonic flow inside the micronozzle. With respect to the 1D model of real nozzle, they overpredicted the performance due to the absence of the strong viscous losses along the depthwise direction. However, they provides useful insight concerning the behavior of the flow inside the microchannel.

6 ACKNOWLEDGEMENTS AND REFERENCES

Special acknowledgment to technical staff of CNR-IMM, Concetta Martucci, Pasquale Creti and Enrico Melissano for microfabrication processes support, to Flavio Casino for wafer bonding setup discussion and realization.

REFERENCES

- [1] M. Silva, D. Guerrieri, A. Cervone, E. Gill, A review of MEMS micropropulsion technologies for cubesats and pocketqubes, *Acta Astronaut.* 143 (2018) 234–243, <https://doi.org/10.1016/j.actaastro.2017.11.049>.
- [2] Y. Gao, Y.F. Ma, J.T. Liu, A review of the vaporizing liquid microthruster technology, in: 2014 ISFMFE – 6th International Symposium on Fluid Machinery and Fluid Engineering, 2014, pp.1–3.
- [3] M. Silva, D. Guerrieri, H. van Zeijl, A. Cervone, E. Gill, Vaporizing liquid microthrusters with integrated heaters and temperature measurement, *Sens. Actuators A, Phys.* 265 (2017) 261–274.
- [4] K. Lemmer, Propulsion for cubesats, *Acta Astronaut.* 134 (2017) 231–243, <https://doi.org/10.1016/j.actaastro.2017.01.048>.
- [5] J. Mueller, W. Tang, A. Wallace, R. Lawton, W. Li, D. Bame, I. Chakraborty, Design, analysis and fabrication of a vaporizing liquid microthruster, in: 33rd Joint Propulsion Conference and Exhibit, 1997, p.3054.
- [6] J. Mueller, D. Bame, I. Chakraborty, A. Wallace, W. Tang, R. Lawton, Proof-of-concept demonstration of a vaporizing liquid micro-thruster, in: 34th AIAA/ASME/SAE/ASEE Joint Propulsion Conference and Exhibit, 1998, p.3924.
- [7] J. Mueller, I. Chakraborty, D. Bame, W. Tang, Vaporizing liquid microthruster concept : preliminary results of initial feasibility studies, in: *Micropropulsion for Small Spacecraft*, Reston, VA, American Institute of Aeronautics and Astronautics, Inc., *Prog. Astronaut. Aeronaut.* 187 (2000) 215–230.
- [8] E. Mukerjee, A. Wallace, K. Yan, D. Howard, R. Smith, S. Collins, Vaporizing liquid microthruster, *Sens. Actuators A, Phys.* 83(1) (2000) 231–236, [https://doi.org/10.1016/S0924-4247\(99\)00389-1](https://doi.org/10.1016/S0924-4247(99)00389-1).
- [9] D. Maurya, S. Das, S. Lahiri, Silicon MEMS vaporizing liquid microthruster with internal microheater, *J. Micromech. Microeng.* 15(5) (2005) 966.
- [10] P. Kundu, T.K. Bhattacharyya, S. Das, Design, fabrication and performance evaluation of a vaporizing liquid microthruster, *J. Micromech. Microeng.* 22(2) (2012) 025016.
- [11] X. Ye, F. Tang, H. Ding, Z. Zhou, Study of a vaporizing water microthruster, *Sens. Actuators A, Phys.* 89(1–2) (2001) 159–165.
- [12] K. Karthikeyan, S. Chou, L. Khoong, Y. Tan, C. Lu, W. Yang, Low temperature co-fired ceramic vaporizing liquid microthruster for microspacecraft applications, *Appl. Energy* 97 (2012) 577–583.
- [13] K. Cheah, K.-S. Low, Fabrication and performance evaluation of a high temperature co-fired ceramic vaporizing liquid microthruster, *J. Micromech. Microeng.* 25(1) (2015) 015013.
- [14] C.-C. Chen, C.-W. Liu, H.-C. Kan, L.-H. Hu, G.-S. Chang, M.-C. Cheng, B.-T. Dai, Simulation and experiment research on vaporizing liquid micro-thruster, *Sens. Actuators A, Phys.* 157(1) (2010) 140–149.

- [15] J. Cen, J. Xu, Performance evaluation and flow visualization of a MEMS based vaporizing liquid micro-thruster, *Acta Astronaut.* 67(3–4) (2010) 468–482, <https://doi.org/10.1016/j.actaastro.2010.04.009>.
- [16] M.G. De Giorgi, D. Fontanarosa, A. Ficarella, Modeling viscous effects on boundary layer of rarefied gas flows inside micronozzles in the slip regime condition, *Energy Proc.* 148 (2018) 838–845.
- [17] Guerrieri, D. C., Silva, M. A., Cervone, A., & Gill, E. (2017). Selection and characterization of green propellants for micro-resistojets. *Journal of Heat Transfer*, 139(10), 102001.
- [18] M.G. De Giorgi, D. Fontanarosa, A novel quasi-one-dimensional model for performance estimation of a Vaporizing Liquid Microthruster, *Aerospace Science and Technology*, Volume 84, 2019, Pages 1020-1034, ISSN 1270-9638, <https://doi.org/10.1016/j.ast.2018.11.039>.
- [19] G.P. Sutton, O. Biblarz, *Rocket Propulsion Elements*, John Wiley & Sons, 2016.
- [20] I.H. Bell, J. Wronski, S. Quoilin, V. Lemort, Pure and pseudo-pure fluid thermophysical property evaluation and the open-source thermophysical property library CoolProp, *Ind. Eng. Chem. Res.* 53(6) (2014) 2498–2508, <https://doi.org/10.1021/ie4033999>.
- [21] C. Tibiriçá, D. Rocha, I.L.S. Sueth Jr., G. Bochio, G. Shimizu, M. Barbosa, S. Ferreira, A complete set of simple and optimized correlations for microchannel flow boiling and two-phase flow applications, *Appl. Therm. Eng.* 126 (2017) 774–795, <https://doi.org/10.1016/j.applthermaleng.2017.07.161>.
- [22] C. Greenshields, H. Weller, L. Gasparini, J. Reese, Implementation of semi-discrete, non-staggered central schemes in a colocated, polyhedral, finite volume framework, for high-speed viscous flows, *Int. J. Numer. Methods Fluids* 63(1) (2010) 1–21, <https://doi.org/10.1002/flid.2069>.